Investigating New Physics Models with Signature of Same-Sign Diboson+$\not{E}_T$

Cheng-Wei Chiang[1,2*], **Sudip Jana**[3†], **Dibyashree Sengupta**[1‡]

[1]*Department of Physics, National Taiwan University, Taipei, Taiwan 10617, R.O.C.*
[2]*Physics Division, National Center for Theoretical Sciences, Taipei, Taiwan 10617, R.O.C.*
[3]*Max-Planck-Institut für Kernphysik, Saupfercheckweg 1, 69117 Heidelberg, Germany*

Abstract

We investigate the prospect of searching for new physics via the novel signature of same-sign diboson + $\not{E}_T$ at current and future LHC. We study three new physics models: (i) natural SUSY models, (ii) type-III seesaw model and (iii) type-II seesaw/Georgi-Machacek model. In the first two class of models, this signature arises due to the presence of a singly-charged particle which has lifetime long enough to escape detection, while in the third model this signature originates resonantly from a doubly-charged particle produced along with two forward jets that, most likely, would escape detection. We analyze in great detail the discovery prospects of the signal in these three classes of models in the current as well as the upcoming runs of the LHC (such as HL-LHC and HE-LHC) by showing a distinction among these scenarios.

---

*E-mail: chengwei@phys.ntu.edu.tw
†E-mail: sudip.jana@mpi-hd.mpg.de
‡E-mail: dsengupta@phys.ntu.edu.tw

arXiv:2106.03888v1 [hep-ph] 7 Jun 2021

1 Introduction

In the past few decades, there have been several major discoveries in particle physics, culminating in the observation of the Higgs boson in 2012 [1, 2]. Despite of this tremendous success of the Standard Model (SM), it is incomplete in its current form. There is strong theoretical as well as experimental evidence (such as the hierarchical pattern seen in the fermion masses and mixings, the origin of neutrino masses, an understanding of dark matter, and the origin of the matter-antimatter asymmetry in the Universe) which calls for new physics beyond the Standard Model (BSM).

At the LHC, several searches have been performed to look for clues of these BSM models. However, we have not seen any clear new physics signals so far. In this work, we investigate the novel signal of same-sign diboson (SSdB) $+ \not{E}_T$ which has been less studied and deserves more attention. This signal is of interest because it has negligibly small background in the SM. Hence, an observation of this signal will give a clear sign of BSM physics. After a careful study, we find that it is possible to observe such a unique signature in three well-motivated BSM scenarios, namely: (i) natural supersymmetry models [3–8], (ii) type-III seesaw model [9], and (iii) type-II seesaw [10–13]/Georgi-Machacek model [14] , while still being consistent with the existing theoretical and experimental limits.

Being a well-motivated BSM framework, supersymmetry (SUSY) provides an elegant solution to the Higgs mass hierarchy problem, accommodates a valid cold dark matter candidate, explains electroweak symmetry breaking, and features gauge coupling unification [15]. Although LHC searches for SUSY particles have pushed their masses (except for higgsinos) to the multi-TeV regime, thereby exposing weak scale SUSY to the risk of being unnatural/highly fine-tuned, there exist a class of SUSY models which can be natural as well as accommodate more massive SUSY particles [1] beyond the reach of the current LHC [16]. These natural SUSY models have a higgsino-like lightest supersymmetric particle (LSP) which under R-parity conservation cannot decay to lighter SM particles, and hence can give rise to the novel SSdB $+ \not{E}_T$ signature via the generic process shown in Fig. 1. Earlier analyses have been done in this regard in Ref. [17, 18]. Our current SUSY analysis differs from these earlier analyses in several aspects to be discussed in detail in Sec. 2.1.

We consider another interesting theoretical framework, type-III seesaw model, which has been proposed [9] to explain the tiny neutrino masses and mixings. In the type-III seesaw model, the SM particle spectrum is extended by three generations of $SU(2)_L$ triplet fermions with hypercharge $Y = 0$, the lightest of which has a lifetime long enough to escape detection [19], provided they have mass around a few hundred GeV. Hence, this model can also give rise to the novel signature of SSdB $+ \not{E}_T$ via the generic process shown in Fig. 1.

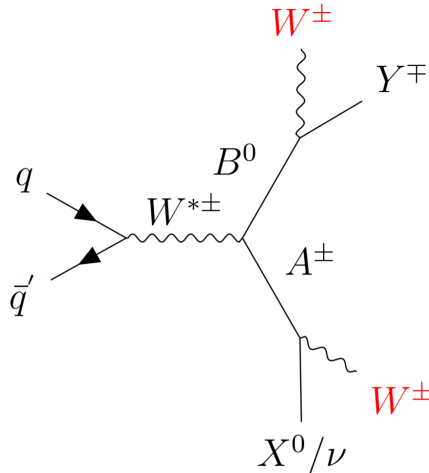[1]Higgsinos are still allowed in the sub-TeV regime.

$W^\pm$

$Y^\mp$

B^0

q

$W^{*\pm}$

$\bar{q}'$

$A^\pm$

$W^\pm$

X^0/ν

Figure 1: A generic Feynman diagram for SSdB + $\not{E}_T$ production at the LHC in BSM models, where B^0, $A^\pm$, X^0 and $Y^\pm$ are new particles.

Another framework that can generate Majorana neutrino mass at tree level is type-II seesaw model [10–13]. In addition to the SM particles, the model is extended by at least one $SU(2)_L$ triplet scalar Δ with hypercharge $Y = 1$. Another model, called Georgi-Machacek (GM) model [14], further has a real $SU(2)_L$ triplet scalar. The doubly-charged scalar from the complex $SU(2)_L$ triplet scalar can be produced via vector boson fusion (VBF) process and decay into two W bosons with same electric charge along with two forward jets coming from the initial state. The forward jets may not be caught by the detector and hence the resultant final state will mimic our signature of interest. However, later in Sec. 2.3, we will show that due to a stringent T-parameter constraint, the type-II seesaw model cannot give a sizeable cross section for this signature, whereas the GM model can.

In this article, we analyze the discovery prospects of the above-mentioned BSM models through the SSdB + $\not{E}_T$ signature at the LHC. We find that the type-II seesaw/GM model can be thus probed at the HL-LHC and that one needs HE-LHC and FCC-hh to probe the natural SUSY models and the type-III seesaw model respectively. The rest of the paper is organized as follows. In Sec. 2, we review the three BSM models and how they give rise to the SSdB + $\not{E}_T$ signature. In Sec. 3, the signals from all the three BSM models are optimized against the SM background. We show how each BSM model stands out for a particular set of cuts and discuss the discovery prospect for each scenario. Finally, we conclude in Sec. 4.

2 SSdB + $\not{E}_T$ Signature from BSM Models

In this section, we briefly review the three classes of new physics models considered in this work, and how each of them leads to the SSdB + $\not{E}_T$ signature at the LHC.

2.1 Supersymmetry

Although weak scale SUSY is a well-motivated BSM framework, experimental searches for SUSY particles have pushed their masses (except for higgsinos) to the multi-TeV regime. For example, current LHC data indicate that $m_{\tilde{g}} > 2.2$ TeV [20] and $m_{\tilde{t}_1} > 1.1$ TeV [21]. Such large lower bounds on the masses of SUSY particles question the naturalness of weak scale SUSY [22]. According to older notions of naturalness, SUSY models with such heavy SUSY particles are highly fine-tuned or unnatural [23–25]. However, these earlier notions of naturalness can be updated to a more conservative electroweak naturalness measure, denoted by Δ_{EW} [26–28]. A numerical expression for Δ_{EW} is obtained from minimizing the minimal supersymmetric standard model (MSSM) scalar potential that equates the Z boson mass to weak scale SUSY parameters as

$$m_Z^2/2 = \frac{m_{H_d}^2 + \Sigma_d^d - (m_{H_u}^2 + \Sigma_u^u)\tan^2\beta}{\tan^2\beta - 1} - \mu^2 \simeq -m_{H_u}^2 - \mu^2 - \Sigma_u^u(\tilde{t}_{1,2}) \ , \qquad (2.1)$$

where μ is the superpotential higgsino mass parameter, $m_{H_u}^2$ and $m_{H_d}^2$ are the soft SUSY breaking up-type and down-type Higgs mass parameters, respectively, $\tan\beta$ is the ratio of up-type Higgs vacuum expectation value (VEV) to the down-type Higgs VEV, and Σ_u^u and Σ_d^d denote radiative corrections as given in the Appendix of Ref. [29]).

Th electroweak naturalness measure, denoted by Δ_{EW}, is defined as

$$\Delta_{EW} = |(\text{max RHS contribution in Eq. (2.1)})|/(m_Z^2/2) \qquad (2.2)$$

It is suggested that a conservative choice for natural SUSY models is $\Delta_{EW} < 30$. Therefore, every point in the parameter space of a SUSY model that yields $\Delta_{EW} < 30$ is considered to be natural. As can be derived from Eq. (2.1) and Eq. (2.2), $\Delta_{EW} < 30$ demands:

- $\mu \sim 100 - 300$ GeV. [2]

- $m_{H_u}^2$ should acquire a small negative value $\sim -(100 - 300)^2$ GeV^2 at the weak scale. This occurs when $m_{H_u}^2$ is driven radiatively from high-energy scales to the weak scale.

- Σ_u^u should also be below $(300)^2$ GeV^2. This is attainable with $m_{\tilde{t}_1} > 1.1$ TeV and $m_{\tilde{g}} > 2.2$ TeV.

Ref. [16] shows several natural SUSY models that satisfy all the above criteria, with huge parameter space still left to be probed experimentally. As seen from the above conditions, natural SUSY models have a unique property that $\mu \ll M_{1,2} < M_3$ where M_1, M_2 and M_3 refer to the masses of bino, wino and gluino, respectively, at the weak scale. Thus, in these natural SUSY models, the LSP is almost purely higgsino-like. Under assumed

---

[2]The space of $\mu < 100$ GeV has been ruled out by LEP2 experiment [30].

R-parity conservation, the LSP becomes a good dark matter candidate in the model and manifests as $\not{E}_T$ in collider experiments. Out of various natural SUSY models listed in Ref. [16], we choose the two extra parameter non-universal Higgs (NUHM2) model [3, 4] with $\mu \ll M_1 < M_2 < M_3$ which can give rise to a clean SSdB + $\not{E}_T$ signature via wino-pair production, as pointed out in Ref. [17, 18]. The corresponding Feynman diagram is shown in Fig. 2.
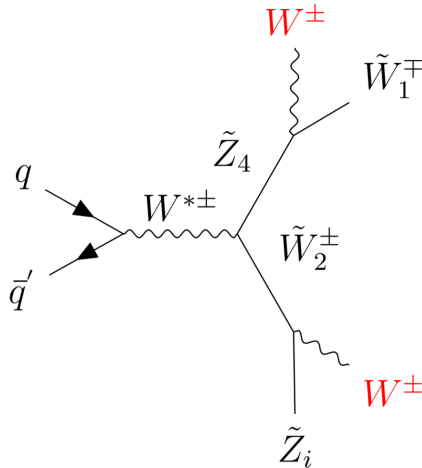

Figure 2: Feynman diagram for SSdB production at the LHC in SUSY models with light higgsinos ($\tilde{W}_1^{\mp}$ and $\tilde{Z}_i$ with $i = 1, 2$). Here $\tilde{Z}_4$ and $\tilde{W}_2^{\pm}$ in the intermediate step are winos.

In this work, we have analyzed this signal in detail using the most up-to-date constraints on $m_{\tilde{g}}$ and $\sigma^{SI}(\tilde{z}_1, p)$ obtained from the LHC data with an integrated luminosity (IL) of 139 fb^{-1} [20] and the XENON1T experiment [31], respectively. The relevant benchmark point is given in Table I. Here we have assumed a more general scenario without gaugino mass unification [32]. This also has the advantage of having the wino mass $\sim$ 770 GeV while satisfying the LHC constraints on gluino mass [20]. Note that the above choice of wino mass is for a comparison of this signal with a similar one obtained from the type-III seesaw model, as discussed in the next subsection.

parameter	NUHM2		parameter	NUHM2
m_0	5000 GeV		$m_{\tilde{\tau}_1}$	4728.91 GeV
$m_{1/2}$	1250 GeV		$m_{\tilde{\tau}_2}$	5061.81 GeV
A_0	-8000 GeV		$m_{\tilde{\nu}_\tau}$	5067.18 GeV
$\tan\beta$	12		$m_{\tilde{w}_1}$	156.56 GeV
M_1(GUT)	1250 GeV		$m_{\tilde{w}_2}$	762.9 GeV
M_2(GUT)	895 GeV		$m_{\tilde{z}_1}$	145.99 GeV
M_3(GUT)	1250 GeV		$m_{\tilde{z}_2}$	157.95 GeV
μ	150 GeV		$m_{\tilde{z}_3}$	559.79 GeV
m_A	2500 GeV		$m_{\tilde{z}_4}$	775.41 GeV
$m_{\tilde{g}}$	2938.23 GeV		m_h	125.09 GeV
$m_{\tilde{u}_L}$	5458.26 GeV		$\Omega^{\text{std}}_{\tilde{z}_1} h^2$	0.007
$m_{\tilde{u}_R}$	5591.07 GeV		$BF(b \to s\gamma) \times 10^4$	3.06
$m_{\tilde{e}_R}$	4840.12 GeV		$BF(B_s \to \mu^+\mu^-) \times 10^9$	3.8
$m_{\tilde{t}_1}$	1820.48 GeV		$\sigma^{SI}(\tilde{z}_1, p)$ (pb)	2.08×10^{-9}
$m_{\tilde{t}_2}$	3925.7 GeV		$\sigma^{SD}(\tilde{z}_1, p)$ (pb)	8.4×10^{-5}
$m_{\tilde{b}_1}$	3959.88 GeV		$\langle\sigma v\rangle\vert_{v\to 0}$ (cm^3/sec)	2.99×10^{-25}
$m_{\tilde{b}_2}$	5301.74 GeV		Δ_{EW}	29.61

Table I: Input parameters and masses for a SUSY benchmark point from the NUHM2 model with $m_t = 173.2$ GeV using `Isajet` 7.88 [33].

2.2 The type-III Seesaw Model

In the type-III seesaw model, the SM particle spectrum is extended by multiple $SU(2)_L$ triplet fermions (Σ's) which have hypercharge $Y = 0$. In order to generate tiny neutrino mass and proper flavor structure in the neutrino sector, one needs to introduce at least two generations of $SU(2)_L$ triplet fermions. The tiny neutrino masses are generated at the tree level and can be expressed as $m_\nu \simeq Y_\nu^2 v^2 / M_\Sigma$, where Y_ν is the Yukawa coupling, v is the SM Higgs VEV, and M_Σ is the triplet fermion mass [9]. In general, the type-III seesaw scenario with $M_\Sigma \simeq \mathcal{O}(1)$ TeV is technically natural and opens up a plethora of implications in collider experiments [19, 34–41].

In our analysis, we consider three generations of $SU(2)_L$ triplet fermions, Σ_i ($i = 1, 2, 3$), with a non-degenerate mass spectrum. The relevant Lagrangian is given by

$$\mathcal{L}_\Sigma = \text{Tr}\left[\overline{\Sigma}_i \slashed{D} \Sigma_i\right] - \left(\frac{1}{2}M_\Sigma^{ij}\text{Tr}\left[\overline{\Sigma^c}_i \Sigma_j\right] + \text{h.c}\right) - \left(\sqrt{2}Y_\Sigma^{ij}\overline{L}_i \Sigma_j H + \text{h.c}\right) , \qquad (2.3)$$

where D_μ is the covariant derivative for Σ_i, M_Σ denotes the triplet fermions mass matrix, and Y_Σ is the Yukawa coupling matrix. For the rest of our paper, we refer to the lightest heavy fermions as $\tilde{\Sigma}$ and their masses as $m_{\tilde{\Sigma}}$. Depending on a normal or inverted hierarchy, the lightest fermion triplet will be Σ_1 or Σ_3, respectively. For simplicity, we set the other two heavy fermions to be almost degenerate.
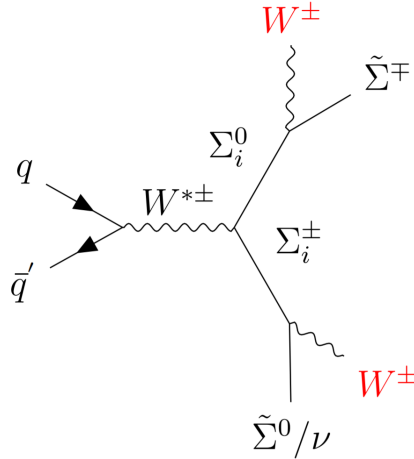

Figure 3: Feynman diagram for the SSdB + $\not{E}_T$ signature at the LHC in the type-III seesaw model, where $\tilde{\Sigma}^0$ and $\tilde{\Sigma}^\pm$ are members of the lightest fermionic triplets.

As can be inferred from a detailed calculation of partial decay widths of these $SU(2)_L$ triplet fermions in Ref. [19], depending on the neutrino parameters, the lightest fermion triplet member $\tilde{\Sigma}^0$ of mass around a few hundred GeV can have lifetime long enough to escape detection and hence shows up as large $\not{E}_T$ in collider experiments. $\tilde{\Sigma}^\pm$, being only a few MeV heavier than its neutral partner $\tilde{\Sigma}^0$, travels a short distance before primarily decaying into $\tilde{\Sigma}^0$ and a charged pion of momentum low enough to be reconstructed as a track. This results in a disappearing track signature from $\tilde{\Sigma}^\pm$ as can also be seen in Ref. [19]. There are several dedicated searches for the disappearing track signature at the LHC [42]. We recast a recent LHC limit in Ref. [42] to derive a bound on the charged heavy fermion in the type-III seesaw model. We find the lower bound on mass of $\tilde{\Sigma}^\pm$ to be around 670 GeV in order to be consistent with the collider data. In our analysis, we set the other two pairs of heavy fermions to have mass at 770 GeV, so that they primarily decay to a $W^\pm$ boson and a $\tilde{\Sigma}^{\pm,0}$ particle through a tiny mixing. This leads to a clean SSdB + $\not{E}_T$ signature from pair production of $\Sigma_i^{\pm,0}$ at the LHC via the Feynman diagram shown in Fig. 3.

2.3   Type-II seesaw/Georgi-Machacek model

In this subsection, we focus on the scenario where the SSdB signature originates from the decay of a doubly-charged scalar. Generally, these doubly-charged scalars appear in

several BSM frameworks [10, 11, 13, 14, 43–59]. One such framework is the simplest type-II seesaw model [10–13] which introduces an $SU(2)_L$ triplet scalar $\Delta = (\Delta^{++}, \Delta^+, \Delta^0)$ with hypercharge $Y = 1$. Tiny neutrino masses are generated while the neutral component of the $SU(2)_L$ triplet, Δ^0, acquires a small VEV, v_Δ. This type of $SU(2)_L$ triplet scalar which contains a doubly-charged scalar Δ^{++} also appears in Minimal Left-Right Symmetric Model [44–46] as well as GM model [14].

At the LHC, these doubly-charged scalars ($\Delta^{\pm\pm}$) can be pair-produced via the Drell-Yan process (s-channel Z/γ exchanges). However, we are focusing on the resonant production of the doubly-charged scalar through the VBF process here, as shown in Fig. 4. This production rate is proportional to v_Δ^2 and becomes more dominant than the Drell-Yan process for $v_\Delta \sim \mathcal{O}(10)$ GeV and $m_{\Delta^{\pm\pm}} \sim \mathcal{O}(100)$ GeV [60, 61]. Note that v_Δ in the simplest type-II seesaw model [10–13] is tightly bounded by the electroweak T parameter, giving $v_\Delta \lesssim 3$ GeV [62]. In the GM model that also contains $SU(2)_L$ scalar triplet fields, ξ with hypercharge $Y = 0$ and χ with hypercharge $Y = 1$, to preserve the custodial symmetry at tree level, v_Δ can be as high as ~ 50 GeV [63, 64]. As a consequence, the resonant production rate could be much larger than in the simplest type-II seesaw scenario.
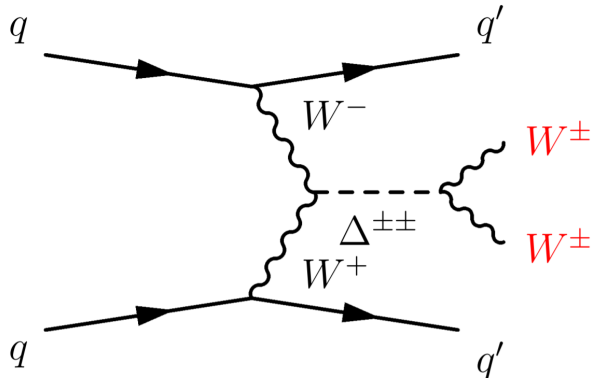

Figure 4: Feynman diagram for SSdB + forward jets production at LHC in the type-II seesaw models.

In general the doubly-charged scalar can be either lightest or heaviest depending on the sign of the quartic coupling in the potential. In the rest of our analysis, we consider the scenario where Δ^{++} is the lightest among all members in the triplet fields. In this scenario, Δ^{++} dominantly decays into same-sign dilepton (SSdL) ($\Delta^{\pm\pm} \to \ell^\pm \ell^\pm$) or SSdB ($\Delta^{\pm\pm} \to W^\pm W^\pm$), depending on the value of v_Δ [65–67]. In Fig. 5, we show a complete decay phase diagram of the doubly-charged scalar of mass 300 GeV. As shown in the plot, $\Delta^{\pm\pm}$ dominantly decays to two same-sign W bosons for $v_\Delta > 10$ MeV, provided the mass splitting $\Delta m \equiv m_{\Delta^{\pm\pm}} - m_{\Delta^\pm}$ is less than 5 GeV. For our analysis, we set the mass splitting $\Delta m = 2$ GeV and $v_\Delta \sim 1$ GeV so that the benchmark point lies in the blue shaded region of Fig. 5 as our region of interest. Thus, after being produced at the LHC along with two

forward jets, $\Delta^{\pm\pm}$ decays primarily to two same-sign W bosons. These jets may escape detection, especially in the forward region with lower detector efficiency. Assuming leptonic decay of the W bosons, we obtain SSdL + $\not{E}_T$ in the final state. In this case, the final state mimics the signature of our interest.
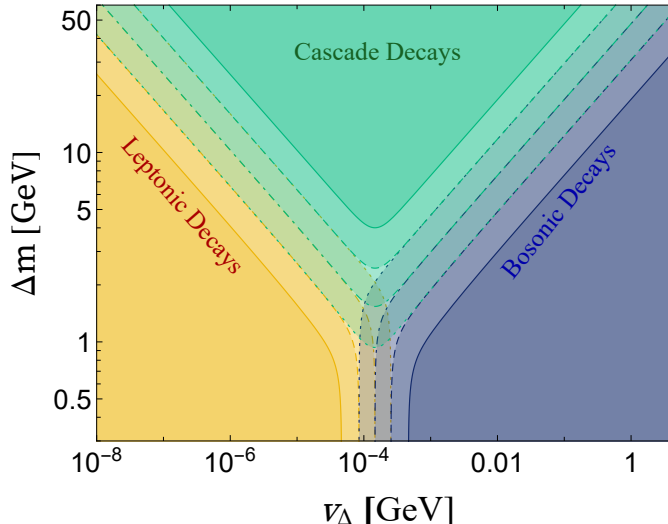

Figure 5: Decay phase diagram of doubly-charged scalar ($\Delta^{\pm\pm}$) with mass = 300 GeV. The solid, dashed, dot-dashed and dotted contours indicate 10%, 50%, 90% and 99% branching ratios respectively, for the bosonic, leptonic or cascade decays. The mass splitting Δm is defined in the main text.

Being proportional to v_Δ^2, the cross section obtained for this signature in the type-II seesaw models, even before any cuts, is negligibly small even for $v_\Delta = 1$ GeV. As stated above, the GM model can accommodate v_Δ as high as 50 GeV. Hence, from now on, we will be considering the GM model, instead of the simplest type-II seesaw model, assuming v_Δ = 10 GeV. The cross section for the stated signal is now sufficiently large to be detectable at the LHC and can scale easily with v_Δ^2.

3 Signal and Background Evaluations

Here in this section we systematically investigate the signal and the background for the aforementioned models. Considering leptonic decays of the W bosons, the signal of interest here has a final state of SSdL + $\not{E}_T$, where the leptons include the electron and muon. As stated in Sec. 2, we can obtain such a signal from wino pair production in NUHM2 model in SUSY, pair production of heavy $SU(2)_L$ triplet in type-III seesaw model, and the resonant production of the doubly-charged scalar in the GM model when the forward jets go undetected. Note that, a final state of SSdL + $\not{E}_T$ can also be obtained from gluino/squark pair production in SUSY models [68–71]. However, this signature can be distinguished

from the signal studied here because the SSdL $+ \not{E}_T$ from gluino/squark pair production appears along with large number of hard central jets. We evaluate the signal from all the three models and the background from the SM, and optimize cuts to efficiently reduce the background. The relevant SM background processes are: $t\bar{t}$, $t\bar{t}t\bar{t}$, $t\bar{t}W^{\pm}$, $t\bar{t}Z$, $W^{\pm}W^{\pm}jj$, $W^{\pm}W^{\pm}W^{\mp}$ and $W^{\pm}Z$.

As discussed in Sec. 2.2, for our analysis the mass of $\tilde{\Sigma}^{\pm,0}$ is taken to be around 670 GeV so as to satisfy the mass constraint in Ref. [42] and we take $\Sigma_i^{\pm,0}$ of mass 770 GeV to ensure that $\Sigma_i^{\pm,0}$ primarily decay to $W^{\pm}$ and $\tilde{\Sigma}^{\pm,0}$. Hence, we take a suitable benchmark point in the NUHM2 model as well, with the wino-like particles ($\tilde{Z}_4$ and $\tilde{W}_2^{\pm}$) also attaining a mass of around 770 GeV, so that the signals from the type-III seesaw model and the NUHM2 model are at par with each other, as stated earlier in Sec. 2.1. However, for the GM model, we have considered $m(\Delta^{\pm\pm}) = 300$ GeV since the limit is less stringent on the mass of $\Delta^{\pm\pm}$ (> 200 GeV [60]) while looking for the bosonic final state signatures at the LHC. Using the same argument, we could have taken lower mass for the wino-like particles ($\tilde{Z}_4$ and $\tilde{W}_2^{\pm}$) in the NUHM2 model but then the NUHM2 benchmark point would not satisfy various constraints such as the mass limit on gluino from the LHC, dark matter constraints from direct detection experiments, etc.

For simulations, we have used `MadGraph` 2.5.5 [72,73] for event generation, interfaced with `Pythia` 8.2 [74] for parton showering and hadronization, followed by `Delphes` 3.4.2 [75] for detector simulation where the default Delphes card is employed. We have used `Isajet` 7.88 [33] to generate the Les Houches Accord (LHA) file for the NUHM2 signal and pass it through the above-mentioned simulation chain.

We have used `Prospino` [76] to calculate the leading-order (LO) and next-to-leading-order (NLO) cross sections for the NUHM2 signal process and type-III seesaw signal process for 14 TeV LHC. Since `Prospino` is designed specifically for calculating NLO cross sections of SUSY processes, using it to calculate the same for the type-III seesaw model is made possible by utilizing the analogy between the type-III seesaw model and the minimal anomaly-mediated SUSY breaking (mAMSB) model [6,77,78]. The mAMSB model has a wino-like LSP ($\tilde{Z}_1$) and a wino-like next-to-LSP (NLSP) ($\tilde{W}_1^{\pm}$), analogous to the type-III seesaw model with its lightest and next-to-lightest particles being $\tilde{\Sigma}^0$ and $\tilde{\Sigma}^{\pm}$, respectively. Thus, a suitable mAMSB parameter space point has been used to calculate the LO and NLO cross sections for the type-III seesaw model.

We have used the K-factor for the type-II seesaw models (and hence the GM model), as done in Ref. [79]. The K-factors for the SM background processes are used as in Ref. [18].

Motivated by the earlier analyses [17,18], we put a set of basic cuts, dubbed the S1-cuts, to reduce the SM backgrounds. Explicitly, the S1-cuts include:

- Require exactly two same-sign isolated leptons, where the isolated leptons are defined as those with $p_T(\ell) > 10$ GeV and $\eta(\ell) < 2.5$.

- Veto events with any identified b-jet.

- Require $p_T(\ell_1) > 20$ GeV, where ℓ_1 denotes the leading lepton.

In the following subsections, we show how each BSM model stands out by further imposing a particular set of additional cuts.

3.1   Supersymmetry Analysis

In the NUHM2 signal, the LSP $\tilde{Z}_1$, due to R-parity conservation, is stable and shows up as $\not{E}_T$ at the LHC. The particles $\tilde{Z}_2$ and $\tilde{W}_1^{\pm}$, being not much heavier than the LSP, are also quasi-stable. Hence the NUHM2 signal has large missing transverse energy ($\not{E}_T$). Similarly, the NUHM2 signal also has large minimum transverse mass ($m_{T_{\min}}$) which is defined as:

$$m_{T_{\min}} = \min(m_T(\ell_1, \not{E}_T), m_T(\ell_2, \not{E}_T)) \tag{3.4}$$

It turns out that we cannot gain a sufficient cross section for $\sqrt{s} = 14$ TeV. Therefore, we extend the analysis to $\sqrt{s} = 27$ TeV. Inspired by the earlier analyses done in this context [17, 18], we further impose the following set of cuts:

- Require $\not{E}_T > 200$ GeV.

- Require $m_{T_{\min}} > 175$ GeV.

Together with the S1-cuts, we call the entire set of cuts as the A1-cuts. After the A1-cuts, we plot the $m_{T_{\min}}$ distribution in Fig. 6.

As suggested by Fig. 6, a cut of $m_{T_{\min}} > 200$ GeV, if employed after the A1-cuts, would result in a cleaner NUHM2 signal with efficiently reduced SM background as well as heavily reduced signal cross sections for the other two BSM models. Therefore, we finally have the A2-cuts:

- A1-cuts + $m_{T_{\min}} > 200$ GeV.

The cut flow is summarized in Table II.

After all the A2-cuts, a sufficient NUHM2 signal cross section is retained, while the SM background and signals from the other two BSM models are greatly reduced. On calculating the significance for an IL of 3 ab^{-1}, the NUHM2 benchmark point yields $S/\sqrt{S+B} = 9.75$ for this signal, while for type-III and GM model we get $S/\sqrt{S+B} = 1.5$ and 0.08, respectively. We have plotted the cluster transverse mass (MCT) distribution and the $\not{E}_T$ distribution after A2-cuts for the total SM background and various signals on top of it in Fig. 7a and Fig. 7b, respectively.
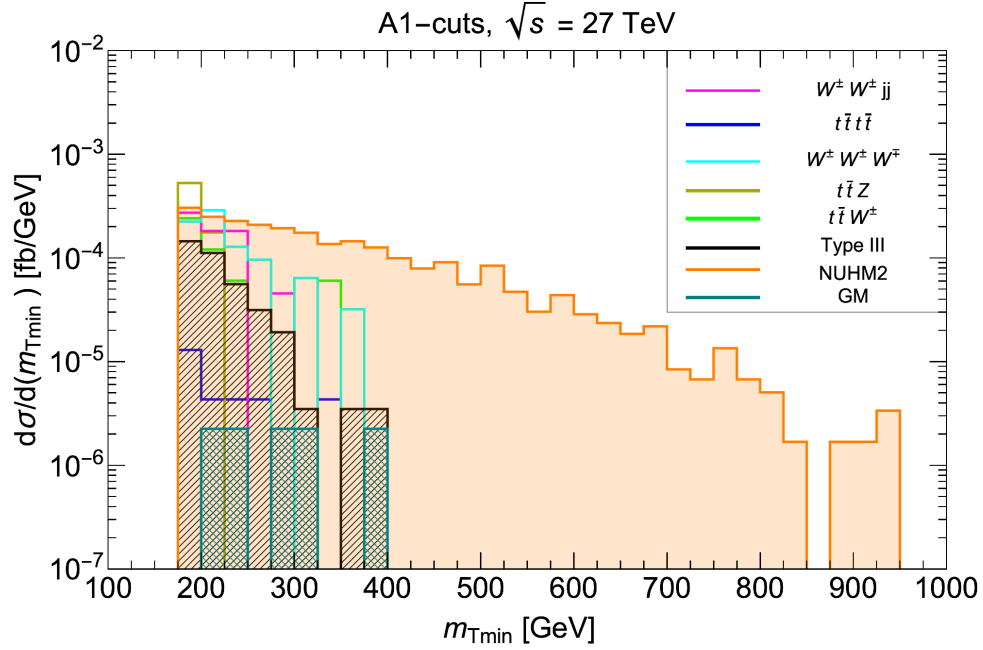
Figure 6: $m_{T_{\min}}$ distribution after A1-cuts.

Process	K-factor	σ (NLO) [ab]	A1 [ab]	A2 [ab]	$\frac{S}{\sqrt{S+B}}$ for 3 ab^{-1}
NUHM2 signal	1.17	$4.2 \cdot 10^4$	60.9	53.3	9.75
type-III signal	1.16	$4.36 \cdot 10^4$	9.33	5.7	1.5
GM signal	1.26	$5.6 \cdot 10^4$	0.28	0.28	0.08
$t\bar{t}$	1.72	$4.1 \cdot 10^9$	0	0	-
$t\bar{t}t\bar{t}$	1.27	$1.1 \cdot 10^5$	0.8	0.4	-
$t\bar{t}W^{\pm}$	1.24	$1.5 \cdot 10^6$	12.1	6.03	-
$t\bar{t}Z$	1.39	$4.4 \cdot 10^6$	17.6	4.4	-
$W^{\pm}W^{\pm}jj$	1.04	$1.1 \cdot 10^6$	17.0	10.2	-
$W^{\pm}W^{\pm}W^{\mp}$	2.45	$8.0 \cdot 10^5$	20.8	15.2	-
$W^{\pm}Z$	1.88	$1.2 \cdot 10^8$	0	0	-
Total BG	−	$4.2 \cdot 10^9$	68.3	36.3	-

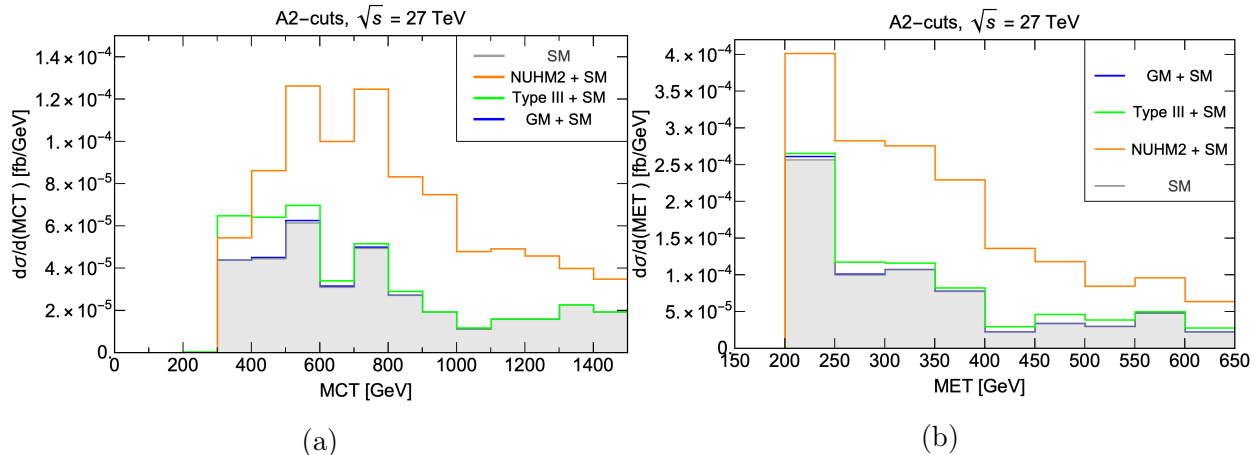Table II: Cut flow table for cleaner NUHM2 signal at $\sqrt{s} = 27$ TeV.

Figure 7: (a) MCT distribution and (b) $\not{E}_T$ distribution after the A2-cuts.

3.2 Type-III Seesaw Analysis

We cannot gain a sufficient cross section for $\sqrt{s} = 14$ TeV for the type-III seesaw signal either, and therefore consider $\sqrt{s} = 27$ TeV. We start with S1-cuts as defined earlier.

It is expected that after the S1-cuts all the SM backgrounds, considered here, should have numerous jets while the type-III seesaw signal can have jets only from initial state QCD radiation. Therefore, requiring only those events that have less than two jets would significantly reduce the SM background while retaining enough type-III seesaw signal.

Similar to the NUHM2 signal, the type-III signal will also show high $\not{E}_T$. However, since in type-III signal, the mass difference between the intermediate state and the final state is not as high as that in the NUHM2 signal, hence the $\not{E}_T$ distribution does not tail out as high as the NUHM2 signal. So, we apply a cut of $\not{E}_T > 100$ GeV, a less stringent cut on $\not{E}_T$ as compared to that applied in case of NUHM2 signal.

For the same reason as mentioned above, we employ a less stringent cut on $m_{T_{\min}}$ as well: a cut of 105 GeV $< m_{T_{\min}} < 195$ GeV. A cut on the upper limit of $m_{T_{\min}}$ has been applied in order to reduce the NUHM2 signal and yet retain most of the type-III signal as for NUHM2 signal the $m_{T_{\min}}$ distribution tails out to a much higher value than that in the type-III signal. The cut on the upper limit of $m_{T_{\min}}$ is thus necessary to differentiate between the NUHM2 and the type-III signal. Therefore after S1-cuts we apply three additional cuts, namely, njet ≤ 1, $\not{E}_T > 100$ GeV and 105 GeV $< m_{T_{\min}} < 195$ GeV and name this entire set of cut as B1-cuts:

- S1-cuts + njet ≤ 1 + $\not{E}_T > 100$ GeV + 105 GeV $< m_{T_{\min}} < 195$ GeV.

After the B1-cuts, the MCT distribution is plotted in Fig. 8 from which we see that a cut of 200 GeV $<$ MCT < 325 GeV can further reduce the SM background and NUHM2

13

signal as well while retaining enough type-III signals to be visible. Therefore next we apply the B2-cuts defined as:
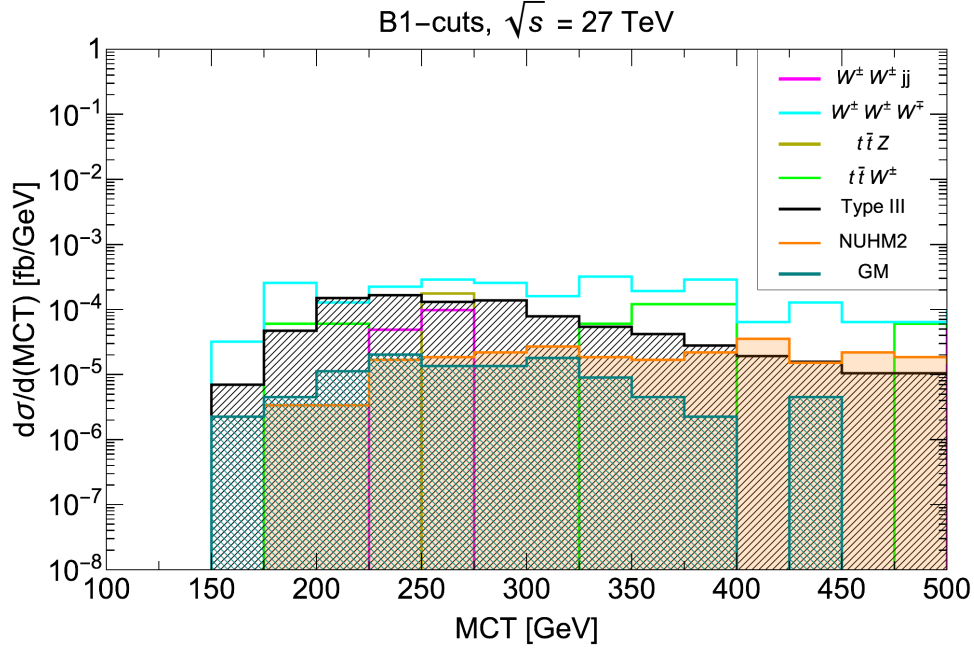
- B1-cuts + 200 GeV < MCT < 325 GeV.

Figure 8: MCT distribution after B1-cuts.

The cut flow for this scenario is summarized in Table III.

Process	K-factor	σ (NLO) [ab]	B1 [ab]	B2 [ab]	$\frac{S}{\sqrt{S+B}}$ for 3 ab^{-1}
NUHM2 signal	1.17	$4.2 \cdot 10^4$	13.2	2.2	0.62
type-III signal	1.16	$4.36 \cdot 10^4$	22.8	16.6	3.97
GM signal	1.26	$5.6 \cdot 10^4$	2.6	1.9	0.54
$t\bar{t}$	1.72	$4.1 \cdot 10^9$	0	0	-
$t\bar{t}t\bar{t}$	1.27	$1.1 \cdot 10^5$	0	0	-
$t\bar{t}W^\pm$	1.24	$1.5 \cdot 10^6$	12.1	1.5	-
$t\bar{t}Z$	1.39	$4.4 \cdot 10^6$	4.4	4.4	-
$W^\pm W^\pm jj$	1.04	$1.1 \cdot 10^6$	4.5	3.4	-
$W^\pm W^\pm W^\mp$	2.45	$8.0 \cdot 10^5$	76.0	26.4	-
$W^\pm Z$	1.88	$1.2 \cdot 10^8$	0	0	-
Total BG	–	$4.2 \cdot 10^9$	97.0	35.7	-

Table III: Cut flow table for cleaner type-III signal at $\sqrt{s} = 27$ TeV.

After the B2-cuts, for an IL of 3 ab^{-1}, we obtain $S/\sqrt{S+B} = 3.97$ for the type-III seesaw signal, $S/\sqrt{S+B} = 0.62$ for the NUHM2 signal and $S/\sqrt{S+B} = 0.54$ for the GM
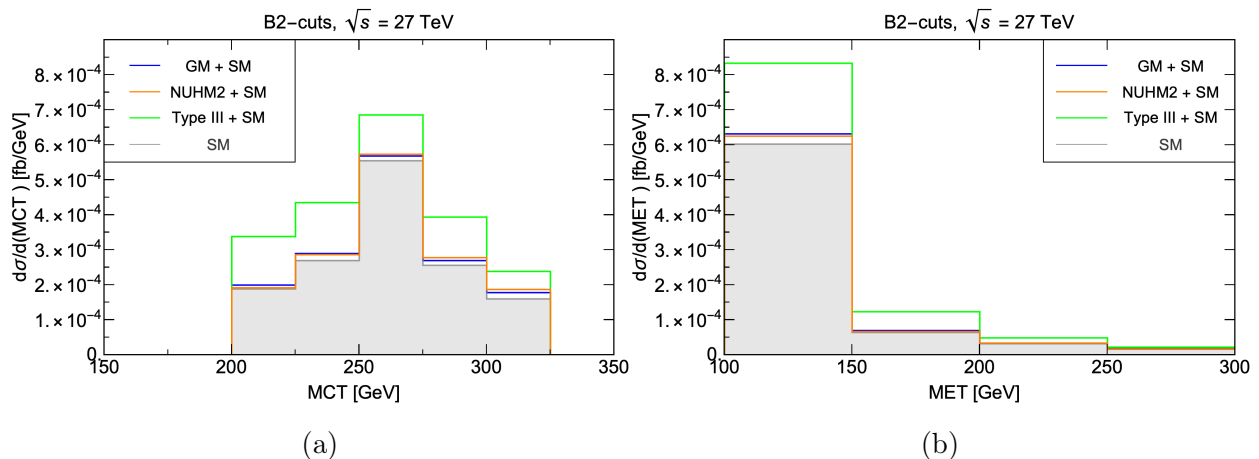
14

Figure 9: (a) MCT distribution and (b) $\not{E}_T$ distribution after the B2-cuts.

model signal. We have plotted the MCT distribution and the $\not{E}_T$ distribution for total SM background and various signals on top of it after imposing the B2-cuts in Fig. 9a and Fig. 9b, respectively. Even for $\sqrt{s} = 27$ TeV, we still cannot reach the 5σ discovery for the type-III seesaw signal. Therefore, a 100 TeV hadron collider (FCC-hh) is called for the type-III seesaw signal.

3.3 Type-II Seesaw/Georgi-Machacek Model Analysis

In the GM model, since the SSdL and $\not{E}_T$ originate from $\Delta^{\pm\pm}$ of mass 300 GeV, the MCT distribution should peak and then sharply fall around 300 GeV. Therefore, an efficient cut after S1-cuts to scoop out the GM model signal would be to require the MCT to be $\leq$ 300 GeV.

Since we explicitly have two forward jets in the GM model signal, hence requiring the number of jets ≥ 2 would be a suitable cut to retain most of the GM model signal. Hence after S1- cuts, we apply two additional cuts, namely, MCT $\leq$ 300 GeV and njet ≥ 2 and this entire set of cut is called the C1-cuts:

- S1-cuts + MCT $\leq$ 300 GeV + njet ≥ 2.

After applying the C1-cuts, we plot the distribution of the pseudorapidity (η) difference between the two leading jets, $\Delta\eta(j_1, j_2)$, in Fig. 10. Due to the presence of two explicit forward jets in the GM model signal, we expect $\Delta\eta(j_1, j_2)$ should peak towards higher values and it indeed peaks around 5 in Fig. 10.

Therefore, requiring $\Delta\eta(j_1, j_2) > 4$ is an extremely efficient cut to not only reduce the SM background but also to almost eliminate the signals from the other two BSM models. We now call this full set of cuts to be the C2-cuts:

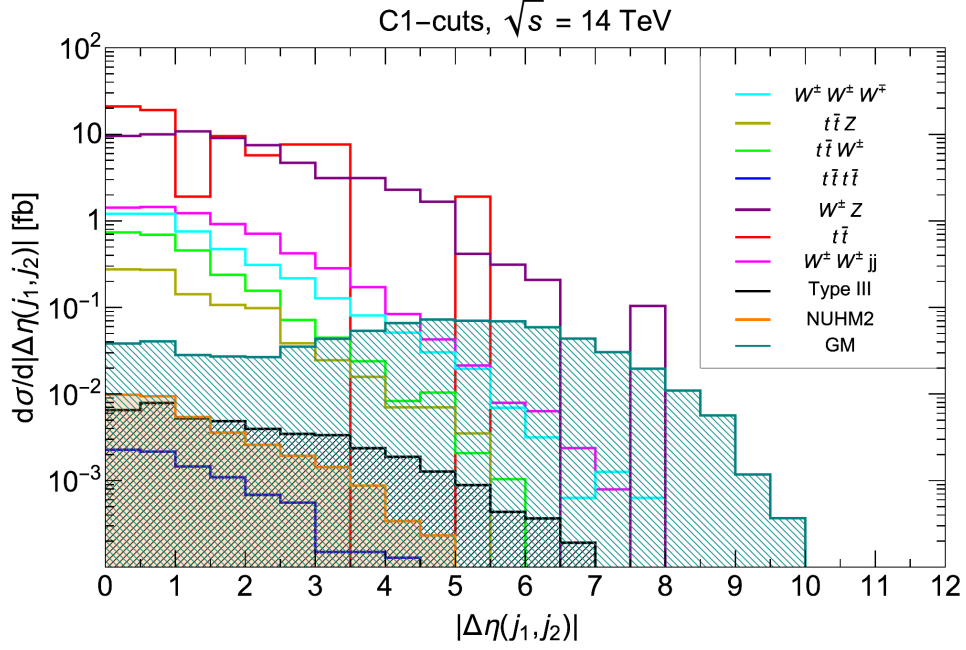- C1-cuts + $\Delta\eta(j_1, j_2) > 4$.

15

Figure 10: $\Delta\eta(j_1, j_2)$ distribution after C1-cuts.

After the C2-cuts, we plot the $\not{E}_T$ distribution shown in Fig. 11. As can be inferred from Fig. 11, a further cut of $\not{E}_T > 150$ GeV will make the largest SM backgrounds $t\bar{t}$ and $W^{\pm}Z$ vanish. We therefore propose the C3-cuts:

- C2-cuts + $\not{E}_T > 150$ GeV.

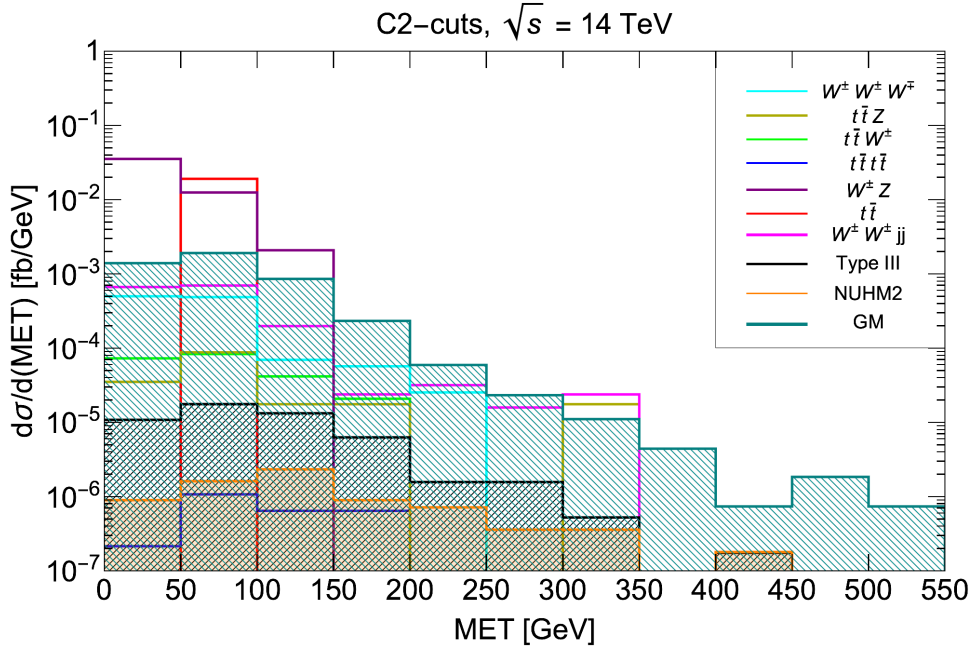

Figure 11: $\not{E}_T$ distribution after C2-cuts.

The cut flow for this scenario is summarized in Table IV.

After all the cuts, we calculate the significance for an IL of 3 ab^{-1} and obtain $S/\sqrt{S+B}$ = 5.4 for the GM model signal, 0.25 for the type-III seesaw signal, and 0.06 for the NUHM2 signal. Thus, with the C3-cuts, the GM model signal can be observed at the 5σ level. In Fig. 12a and Fig. 12b, we show the MCT distribution and the $\not{E}_T$ distribution after the C3-cuts for the total SM background and the various signals on top of it, respectively.

Process	K-factor	σ (NLO) [ab]	C1 [ab]	C2 [ab]	C3 [ab]	$\frac{S}{\sqrt{S+B}}$ for 3 ab^{-1}
NUHM2 signal	1.17	$8.95 \cdot 10^3$	17.91	0.4	0.12	0.06
type-III signal	1.16	$8.71 \cdot 10^3$	21.4	2.6	0.5	0.25
GM signal	1.26	$1.84 \cdot 10^4$	371.1	224.5	16.7	5.4
$t\bar{t}$	1.72	$9.5 \cdot 10^8$	$3.7 \cdot 10^4$	953.1	0	-
$t\bar{t}t\bar{t}$	1.27	$1.1 \cdot 10^4$	4.4	0.13	0.03	-
$t\bar{t}W^\pm$	1.24	$5.2 \cdot 10^5$	$1.22 \cdot 10^3$	11.0	1.04	-
$t\bar{t}Z$	1.39	$8.8 \cdot 10^5$	495.6	8.8	1.8	-
$W^\pm W^\pm jj$	1.04	$3.9 \cdot 10^5$	$3.4 \cdot 10^3$	83.0	4.8	-
$W^\pm W^\pm W^\mp$	2.45	$3.2 \cdot 10^5$	$2.25 \cdot 10^3$	56.9	4.1	-
$W^\pm Z$	1.88	$5.2 \cdot 10^7$	$3.1 \cdot 10^4$	$2.5 \cdot 10^3$	0	-
Total BG	$-$	$1.01 \cdot 10^9$	$7.6 \cdot 10^4$	$3.6 \cdot 10^3$	11.77	-

Table IV: Cut flow table for cleaner GM model signal at $\sqrt{s} = 14$ TeV.
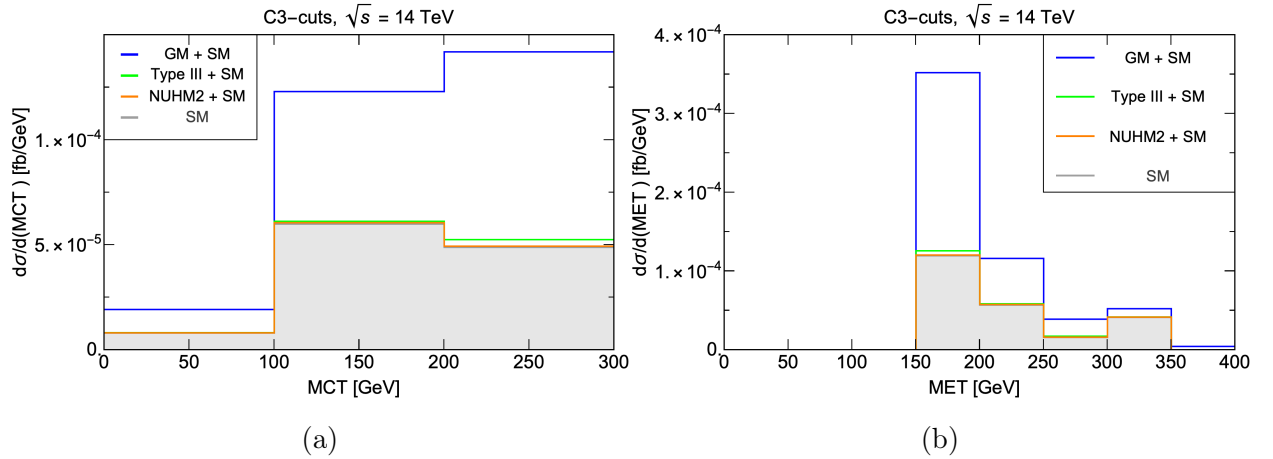

Figure 12: (a) MCT distribution and (b) $\not{E}_T$ distribution after C3-cuts.

Note that, it has been possible to observe the GM model signal with 5σ significance at HL-LHC while for NUHM2 signal one needs HE-LHC and for type-III seesaw signal one needs 100 TeV collider to obtain 5σ significance because $m(\Delta^{\pm\pm})$ in GM model is much less than $m(\Sigma_i^\pm)$ in type-III seesaw and $m(\tilde{Z}_4, \tilde{W}_2^\pm)$ in NUHM2 model. Since the GM model

17

signal is produced via VBF process, hence taking $m(\Delta^{\pm\pm}) \sim m(\Sigma_i^{\pm}) \sim 770$ GeV, would yield much lower cross-section and one might need to upgrade to HE-LHC to obtain 5σ significance even for GM model signal. However, we have taken $m(\Delta^{\pm\pm}) = 300$ GeV (*not* at par with the mass of intermediate states in the other two new physics model signature) in order to highlight the fact that experimental limits on $m(\Delta^{\pm\pm})$ do allow us to obtain a 5σ significance at HL-LHC for GM model signal while experimental mass constraints compel us to upgrade to higher energies to obtain 5σ significance for NUHM2 and type-III seesaw signal.

4 Conclusions

In this paper, we focus on using the signature of SSdB + $\not{E}_T$ to search for new physics and study how various models with such a signature can be distinguished by imposing suitable cuts. To reduce the SM background, we consider leptonic decays of the diboson, yielding SSdL + $\not{E}_T$ in the final state. We have analyzed three new physics models: the NUHM2 scenario of natural SUSY models, the type-III seesaw model, and the GM model. We carefully select the imposed cuts for each model to obtain a sufficiently large significance for its signal. Assuming an IL of 3 ab^{-1} and $\sqrt{s} = 14$ TeV, the C3-cuts are needed to observe a clean GM model signal at a level above 5σ significance. For the NUHM2 model, the A2-cuts should be used for data collected from an IL of 3 ab^{-1} and $\sqrt{s} = 27$ TeV. Finally, the type-III signal does not yield enough significance at both $\sqrt{s} = 14$ TeV and 27 TeV for an IL of 3 ab^{-1}. In this case, we will need a 100-TeV hadron collider to observe a clean signal in the SSdL + $\not{E}_T$ channel.

Acknowledgments

References

[1] **ATLAS** Collaboration, G. Aad *et al.*, "Observation of a new particle in the search for the Standard Model Higgs boson with the ATLAS detector at the LHC," *Phys. Lett. B* **716** (2012) 1–29, arXiv:1207.7214 [hep-ex].

[2] **CMS** Collaboration, S. Chatrchyan *et al.*, "Observation of a New Boson at a Mass of 125 GeV with the CMS Experiment at the LHC," *Phys. Lett. B* **716** (2012) 30–61, `arXiv:1207.7235 [hep-ex]`.

[3] D. Matalliotakis and H. P. Nilles, "Implications of nonuniversality of soft terms in supersymmetric grand unified theories," *Nucl. Phys. B* **435** (1995) 115–128, `arXiv:hep-ph/9407251`.

[4] H. Baer, A. Mustafayev, S. Profumo, A. Belyaev, and X. Tata, "Direct, indirect and collider detection of neutralino dark matter in SUSY models with non-universal Higgs masses," *JHEP* **07** (2005) 065, `arXiv:hep-ph/0504001`.

[5] H. Baer, V. Barger, H. Serce, and X. Tata, "Natural generalized mirage mediation," *Phys. Rev. D* **94** no. 11, (2016) 115017, `arXiv:1610.06205 [hep-ph]`.

[6] L. Randall and R. Sundrum, "Out of this world supersymmetry breaking," *Nucl. Phys. B* **557** (1999) 79–118, `arXiv:hep-th/9810155`.

[7] H. Baer, V. Barger, and D. Sengupta, "Anomaly mediated SUSY breaking model retrofitted for naturalness," *Phys. Rev. D* **98** no. 1, (2018) 015039, `arXiv:1801.09730 [hep-ph]`.

[8] H. Baer, V. Barger, S. Salam, D. Sengupta, and K. Sinha, "Status of weak scale supersymmetry after LHC Run 2 and ton-scale noble liquid WIMP searches," *Eur. Phys. J. ST* **229** no. 21, (2020) 3085–3141, `arXiv:2002.03013 [hep-ph]`.

[9] R. Foot, H. Lew, X. G. He, and G. C. Joshi, "Seesaw Neutrino Masses Induced by a Triplet of Leptons," *Z. Phys. C* **44** (1989) 441.

[10] M. Magg and C. Wetterich, "Neutrino Mass Problem and Gauge Hierarchy," *Phys. Lett. B* **94** (1980) 61–64.

[11] J. Schechter and J. W. F. Valle, "Neutrino Masses in SU(2) x U(1) Theories," *Phys. Rev. D* **22** (1980) 2227.

[12] R. N. Mohapatra and G. Senjanovic, "Neutrino Mass and Spontaneous Parity Nonconservation," *Phys. Rev. Lett.* **44** (1980) 912.

[13] G. Lazarides, Q. Shafi, and C. Wetterich, "Proton Lifetime and Fermion Masses in an SO(10) Model," *Nucl. Phys. B* **181** (1981) 287–300.

[14] H. Georgi and M. Machacek, "DOUBLY CHARGED HIGGS BOSONS," *Nucl. Phys. B* **262** (1985) 463–477.

19

[15] H. Baer and X. Tata, *Weak scale supersymmetry: From superfields to scattering events.* Cambridge University Press, 5, 2006.

[16] H. Baer, V. Barger, J. S. Gainer, D. Sengupta, H. Serce, and X. Tata, "LHC luminosity and energy upgrades confront natural supersymmetry models," *Phys. Rev. D* **98** no. 7, (2018) 075010, `arXiv:1808.04844 [hep-ph]`.

[17] H. Baer, V. Barger, P. Huang, D. Mickelson, A. Mustafayev, W. Sreethawong, and X. Tata, "Same sign diboson signature from supersymmetry models with light higgsinos at the LHC," *Phys. Rev. Lett.* **110** no. 15, (2013) 151801, `arXiv:1302.5816 [hep-ph]`.

[18] H. Baer, V. Barger, J. S. Gainer, M. Savoy, D. Sengupta, and X. Tata, "Aspects of the same-sign diboson signature from wino pair production with light higgsinos at the high luminosity LHC," *Phys. Rev. D* **97** no. 3, (2018) 035012, `arXiv:1710.09103 [hep-ph]`.

[19] S. Jana, N. Okada, and D. Raut, "Displaced Vertex and Disappearing Track Signatures in type-III Seesaw," `arXiv:1911.09037 [hep-ph]`.

[20] **ATLAS** Collaboration, M. Aaboud *et al.*, "Search for squarks and gluinos in final states with jets and missing transverse momentum using 36 fb^{-1} of $\sqrt{s} = 13$ TeV pp collision data with the ATLAS detector," *Phys. Rev. D* **97** no. 11, (2018) 112001, `arXiv:1712.02332 [hep-ex]`.

[21] **ATLAS, CMS** Collaboration, T. A. Vami, "Searches for gluinos and squarks," *PoS* **LHCP2019** (2019) 168, `arXiv:1909.11753 [hep-ex]`.

[22] N. Craig, "The State of Supersymmetry after Run I of the LHC," in *Beyond the Standard Model after the first run of the LHC.* 9, 2013. `arXiv:1309.0528 [hep-ph]`.

[23] R. Barbieri and G. F. Giudice, "Upper Bounds on Supersymmetric Particle Masses," *Nucl. Phys. B* **306** (1988) 63–76.

[24] M. Papucci, J. T. Ruderman, and A. Weiler, "Natural SUSY Endures," *JHEP* **09** (2012) 035, `arXiv:1110.6926 [hep-ph]`.

[25] R. Kitano and Y. Nomura, "Supersymmetry, naturalness, and signatures at the LHC," *Phys. Rev. D* **73** (2006) 095004, `arXiv:hep-ph/0602096`.

[26] H. Baer, V. Barger, and D. Mickelson, "How conventional measures overestimate electroweak fine-tuning in supersymmetric theory," *Phys. Rev. D* **88** no. 9, (2013) 095013, `arXiv:1309.2984 [hep-ph]`.

[27] A. Mustafayev and X. Tata, "Supersymmetry, Naturalness, and Light Higgsinos," *Indian J. Phys.* **88** (2014) 991–1004, arXiv:1404.1386 [hep-ph].

[28] H. Baer, V. Barger, D. Mickelson, and M. Padeffke-Kirkland, "SUSY models under siege: LHC constraints and electroweak fine-tuning," *Phys. Rev. D* **89** no. 11, (2014) 115019, arXiv:1404.2277 [hep-ph].

[29] H. Baer, V. Barger, P. Huang, D. Mickelson, A. Mustafayev, and X. Tata, "Radiative natural supersymmetry: Reconciling electroweak fine-tuning and the Higgs boson mass," *Phys. Rev. D* **87** no. 11, (2013) 115028, arXiv:1212.2655 [hep-ph].

[30] **LEP, ALEPH, DELPHI, L3, OPAL, LEP Electroweak Working Group, SLD Electroweak Group, SLD Heavy Flavor Group** Collaboration, t. S. Electroweak, "A Combination of preliminary electroweak measurements and constraints on the standard model," arXiv:hep-ex/0312023.

[31] **XENON** Collaboration, E. Aprile *et al.*, "First Dark Matter Search Results from the XENON1T Experiment," *Phys. Rev. Lett.* **119** no. 18, (2017) 181301, arXiv:1705.06655 [astro-ph.CO].

[32] H. Baer, V. Barger, P. Huang, D. Mickelson, M. Padeffke-Kirkland, and X. Tata, "Natural SUSY with a bino- or wino-like LSP," *Phys. Rev. D* **91** no. 7, (2015) 075005, arXiv:1501.06357 [hep-ph].

[33] F. E. Paige, S. D. Protopopescu, H. Baer, and X. Tata, "ISAJET 7.69: A Monte Carlo event generator for pp, anti-p p, and e+e- reactions," arXiv:hep-ph/0312045.

[34] R. Franceschini, T. Hambye, and A. Strumia, "Type-III see-saw at LHC," *Phys. Rev. D* **78** (2008) 033002, arXiv:0805.1613 [hep-ph].

[35] A. Arhrib, B. Bajc, D. K. Ghosh, T. Han, G.-Y. Huang, I. Puljak, and G. Senjanovic, "Collider Signatures for Heavy Lepton Triplet in Type I+III Seesaw," *Phys. Rev. D* **82** (2010) 053004, arXiv:0904.2390 [hep-ph].

[36] P. Bandyopadhyay, S. Choi, E. J. Chun, and K. Min, "Probing Higgs bosons via the type III seesaw mechanism at the LHC," *Phys. Rev. D* **85** (2012) 073013, arXiv:1112.3080 [hep-ph].

[37] D. Goswami and P. Poulose, "Direct searches of Type III seesaw triplet fermions at high energy e^+e^- collider," *Eur. Phys. J. C* **78** no. 1, (2018) 42, arXiv:1702.07215 [hep-ph].

[38] S. Ashanujjaman and K. Ghosh, "Type-III Seesaw: Phenomenological Implications of the Information Lost in Decoupling from High-Energy to Low-Energy," arXiv:2102.09536 [hep-ph].

[39] A. Das and S. Mandal, "Bounds on the triplet fermions in type-III seesaw and implications for collider searches," *Nucl. Phys. B* **966** (2021) 115374, arXiv:2006.04123 [hep-ph].

[40] C. Biggio, E. Fernandez-Martinez, M. Filaci, J. Hernandez-Garcia, and J. Lopez-Pavon, "Global Bounds on the Type-III Seesaw," *JHEP* **05** (2020) 022, arXiv:1911.11790 [hep-ph].

[41] F. del Aguila and J. A. Aguilar-Saavedra, "Distinguishing seesaw models at LHC with multi-lepton signals," *Nucl. Phys. B* **813** (2009) 22–90, arXiv:0808.2468 [hep-ph].

[42] **CMS** Collaboration, A. M. Sirunyan *et al.*, "Search for disappearing tracks in proton-proton collisions at $\sqrt{s} = 13$ TeV," *Phys. Lett. B* **806** (2020) 135502, arXiv:2004.05153 [hep-ex].

[43] R. N. Mohapatra and G. Senjanovic, "Neutrino Masses and Mixings in Gauge Models with Spontaneous Parity Violation," *Phys. Rev. D* **23** (1981) 165.

[44] J. C. Pati and A. Salam, "Lepton Number as the Fourth Color," *Phys. Rev. D* **10** (1974) 275–289. [Erratum: Phys.Rev.D 11, 703–703 (1975)].

[45] R. N. Mohapatra and J. C. Pati, "Left-Right Gauge Symmetry and an Isoconjugate Model of CP Violation," *Phys. Rev. D* **11** (1975) 566–571.

[46] G. Senjanovic and R. N. Mohapatra, "Exact Left-Right Symmetry and Spontaneous Violation of Parity," *Phys. Rev. D* **12** (1975) 1502.

[47] R. Kuchimanchi and R. N. Mohapatra, "No parity violation without R-parity violation," *Phys. Rev. D* **48** (1993) 4352–4360, arXiv:hep-ph/9306290.

[48] K. S. Babu and R. N. Mohapatra, "Minimal Supersymmetric Left-Right Model," *Phys. Lett. B* **668** (2008) 404–409, arXiv:0807.0481 [hep-ph].

[49] K. S. Babu and A. Patra, "Higgs Boson Spectra in Supersymmetric Left-Right Models," *Phys. Rev. D* **93** no. 5, (2016) 055030, arXiv:1412.8714 [hep-ph].

[50] L. Basso, B. Fuks, M. E. Krauss, and W. Porod, "Doubly-charged Higgs and vacuum stability in left-right supersymmetry," *JHEP* **07** (2015) 147, arXiv:1503.08211 [hep-ph].

[51] A. Zee, "Quantum Numbers of Majorana Neutrino Masses," *Nucl. Phys. B* **264** (1986) 99–110.

[52] K. S. Babu, "Model of 'Calculable' Majorana Neutrino Masses," *Phys. Lett. B* **203** (1988) 132–136.

[53] N. Arkani-Hamed, A. G. Cohen, E. Katz, A. E. Nelson, T. Gregoire, and J. G. Wacker, "The Minimal moose for a little Higgs," *JHEP* **08** (2002) 021, arXiv:hep-ph/0206020.

[54] K. S. Babu, P. S. B. Dev, S. Jana, and A. Thapa, "Unified framework for B-anomalies, muon $g2$ and neutrino masses," *JHEP* **03** (2021) 179, arXiv:2009.01771 [hep-ph].

[55] J. F. Gunion, R. Vega, and J. Wudka, "Higgs triplets in the standard model," *Phys. Rev. D* **42** (1990) 1673–1691.

[56] K. S. Babu, S. Nandi, and Z. Tavartkiladze, "New Mechanism for Neutrino Mass Generation and Triply Charged Higgs Bosons at the LHC," *Phys. Rev. D* **80** (2009) 071702, arXiv:0905.2710 [hep-ph].

[57] F. Bonnet, D. Hernandez, T. Ota, and W. Winter, "Neutrino masses from higher than d=5 effective operators," *JHEP* **10** (2009) 076, arXiv:0907.3143 [hep-ph].

[58] S. Bhattacharya, S. Jana, and S. Nandi, "Neutrino Masses and Scalar Singlet Dark Matter," *Phys. Rev. D* **95** no. 5, (2017) 055003, arXiv:1609.03274 [hep-ph].

[59] K. Kumericki, I. Picek, and B. Radovcic, "TeV-scale Seesaw with Quintuplet Fermions," *Phys. Rev. D* **86** (2012) 013006, arXiv:1204.6599 [hep-ph].

[60] C.-W. Chiang, T. Nomura, and K. Tsumura, "Search for doubly charged Higgs bosons using the same-sign diboson mode at the LHC," *Phys. Rev. D* **85** (2012) 095023, arXiv:1202.2014 [hep-ph].

[61] C.-W. Chiang, A.-L. Kuo, and T. Yamada, "Searches of exotic Higgs bosons in general mass spectra of the Georgi-Machacek model at the LHC," *JHEP* **01** (2016) 120, arXiv:1511.00865 [hep-ph].

[62] **Particle Data Group** Collaboration, P. A. Zyla *et al.*, "Review of Particle Physics," *PTEP* **2020** no. 8, (2020) 083C01.

[63] S. Blasi, S. De Curtis, and K. Yagyu, "Effects of custodial symmetry breaking in the Georgi-Machacek model at high energies," *Phys. Rev. D* **96** no. 1, (2017) 015001, arXiv:1704.08512 [hep-ph].

[64] C.-W. Chiang, A.-L. Kuo, and K. Yagyu, "One-loop renormalized Higgs boson vertices in the Georgi-Machacek model," *Phys. Rev. D* **98** no. 1, (2018) 013008, `arXiv:1804.02633 [hep-ph]`.

[65] A. Melfo, M. Nemevsek, F. Nesti, G. Senjanovic, and Y. Zhang, "Type II Seesaw at LHC: The Roadmap," *Phys. Rev. D* **85** (2012) 055018, `arXiv:1108.4416 [hep-ph]`.

[66] M. Aoki, S. Kanemura, and K. Yagyu, "Testing the Higgs triplet model with the mass difference at the LHC," *Phys. Rev. D* **85** (2012) 055007, `arXiv:1110.4625 [hep-ph]`.

[67] C.-W. Chiang and K. Yagyu, "Testing the custodial symmetry in the Higgs sector of the Georgi-Machacek model," *JHEP* **01** (2013) 026, `arXiv:1211.2658 [hep-ph]`.

[68] R. M. Barnett, J. F. Gunion, and H. E. Haber, "LIKE SIGN DILEPTONS AS A SIGNAL FOR GLUINO PRODUCTION," in *1988 DPF Summer Study on High-energy Physics in the 1990s (Snowmass 88)*. 10, 1988.

[69] H. Baer, X. Tata, and J. Woodside, "Gluino Cascade Decay Signatures at the Tevatron Collider," *Phys. Rev. D* **41** (1990) 906–915.

[70] H. Baer, X. Tata, and J. Woodside, "Multi - lepton signals from supersymmetry at hadron super colliders," *Phys. Rev. D* **45** (1992) 142–160.

[71] R. M. Barnett, J. F. Gunion, and H. E. Haber, "Discovering supersymmetry with like sign dileptons," *Phys. Lett. B* **315** (1993) 349–354, `arXiv:hep-ph/9306204`.

[72] J. Alwall, M. Herquet, F. Maltoni, O. Mattelaer, and T. Stelzer, "MadGraph 5 : Going Beyond," *JHEP* **06** (2011) 128, `arXiv:1106.0522 [hep-ph]`.

[73] J. Alwall, R. Frederix, S. Frixione, V. Hirschi, F. Maltoni, O. Mattelaer, H. S. Shao, T. Stelzer, P. Torrielli, and M. Zaro, "The automated computation of tree-level and next-to-leading order differential cross sections, and their matching to parton shower simulations," *JHEP* **07** (2014) 079, `arXiv:1405.0301 [hep-ph]`.

[74] T. Sjöstrand, S. Ask, J. R. Christiansen, R. Corke, N. Desai, P. Ilten, S. Mrenna, S. Prestel, C. O. Rasmussen, and P. Z. Skands, "An introduction to PYTHIA 8.2," *Comput. Phys. Commun.* **191** (2015) 159–177, `arXiv:1410.3012 [hep-ph]`.

[75] **DELPHES 3** Collaboration, J. de Favereau, C. Delaere, P. Demin, A. Giammanco, V. Lemaître, A. Mertens, and M. Selvaggi, "DELPHES 3, A modular framework for fast simulation of a generic collider experiment," *JHEP* **02** (2014) 057, `arXiv:1307.6346 [hep-ex]`.

[76] W. Beenakker, R. Hopker, and M. Spira, "PROSPINO: A Program for the production of supersymmetric particles in next-to-leading order QCD," `arXiv:hep-ph/9611232`.

[77] T. Gherghetta, G. F. Giudice, and J. D. Wells, "Phenomenological consequences of supersymmetry with anomaly induced masses," *Nucl. Phys. B* **559** (1999) 27–47, `arXiv:hep-ph/9904378`.

[78] J. L. Feng and T. Moroi, "Supernatural supersymmetry: Phenomenological implications of anomaly mediated supersymmetry breaking," *Phys. Rev. D* **61** (2000) 095004, `arXiv:hep-ph/9907319`.

[79] **ATLAS** Collaboration, "Search for doubly-charged Higgs bosons in same-charge electron pair final states using proton-proton collisions at $\sqrt{s} = 13\,\text{TeV}$ with the ATLAS detector,".